Available online at www.sciencedirect.com
ScienceDirect
Journal of Applied Geophysics 63 (2007) 13–23
JOURNAL OF APPLIED GEOPHYSICS
www.elsevier.com/locate/jappgeo

Prediction of the effects of soil and target properties on the antipersonnel landmine detection performance of ground-penetrating radar: A Colombian case study

Olga Lopera [a,b,c,*], Nada Milisavljevic [a]

[a] Signal and Image Centre, Royal Military Academy, Av. renaissance 30, 1000 Brussels, Belgium
[b] Department of Electrical and Electronic Eng., University of Los Andes, Bogota, Colombia
[c] Telecommunications Laboratory, Catholic University of Louvain, Louvain-la-neuve, Belgium

Received 10 November 2005; accepted 22 February 2007

Abstract

The performance of ground-penetrating (GPR) radar is determined fundamentally by the soil electromagnetic (EM) properties and the target characteristics. In this paper, we predict the effects of such properties on the antipersonnel (AP) landmine detection performance of GPR in a Colombian scenario. Firstly, we use available soil geophysical information in existing pedotransfer models to calculate soil EM properties. The latter are included in a two-dimensional (2D), finite-difference time-domain (FDTD) modeling program in conjunction with the characteristics of AP landmines to calculate the buried target reflection. The approach is applied to two soils selected among Colombian mine-affected areas, and several local improvised explosive devices (IEDs) and AP landmines are modeled as targets. The signatures from such targets buried in the selected soils are predicted, considering different conditions. Finally, we show how the GPR can contribute in detecting low- and non-metallic targets in these Colombian soils. Such a system could be quite adequate for complementing humanitarian landmine detection by metal detectors.

Keywords: Ground-penetrating radar; Detection performance; Pedotransfer functions; FDTD modeling; Humanitarian demining

1. Introduction

In 2004, statistics of landmine victims ranked Colombia as the third most heavily mine-affected country in the world with 812 casualties. Nowadays, it is estimated that more than one hundred thousand antipersonnel (AP) landmines are buried across 422 municipalities, which constitutes 40% of the national territory (ICBL, 2005).[1] These are American and Belgian manufactured landmines, as well as landmines manufactured by the Colombian Military Industry (INDUMIL). However, a considerable number is made in an artisan way by the guerrillas (*e.g.*, FARC and ELN[2]). These low cost landmines are called *improvised explosive devices* (IEDs). Although the Colombian

* Corresponding author. Signal and Image Centre, Royal Military Academy, Av. renaissance 30, 1000 Brussels, Belgium. Tel.: +32 2742 6666; fax: +32 2737 6472.
E-mail address: olopera@elec.rma.ac.be (O. Lopera).

0926-9851/$ - see front matter © 2007 Elsevier B.V. All rights reserved.
doi:10.1016/j.jappgeo.2007.02.002

[1] International Campaign to Ban Landmines, ICBL.
[2] Fuerzas Armadas Revolucionarias de Colombia — FARC, Ejercito de Liberacion Nacional — ELN.

government ratified the Ottawa Convention in 2001, the guerrillas still place IEDs across the country. The Explosive Devices Manipulation Unit (MARTE) of the National Military Forces is the most expert group in mine-clearing works in Colombia. They use classical demining procedures, namely, electromagnetic (EM) induction methods (metal detector, MD). However, MDs do not reliably detect plastic, low-metallic landmines[3] in a post-conflict area contaminated by grenade fragments, cartridges, and other metallic materials buried premeditatedly to confuse the deminers. Besides the fact that some Colombian mined areas contain ferruginous soils (*i.e.* with a high iron content) which adversely affects the sensibility of EM induction methods, a significant amount of IEDs contain only plastic and other non-metallic elements. When demining is performed using a MD, all these factors increase the probability of having an accident up to 40%.[4] Therefore, additional sensors for complementing the MD are required in mine-affected areas with difficult conditions such as those in Colombia.

Several sensors for landmine detection have been proposed and utilized worldwide (MacDonald et al., 2003). Among these, ground-penetrating radar (GPR) is considered as a promising technology, because of its ability to detect both metallic and non-metallic AP landmines by non-invasive subsurface sensing (Bruschini et al., 1998; Carin et al., 1999; Gao et al., 2000; Chen et al., 2001; Scheers, 2001; Roth, 2004; Daniels, 2004). It is well known that the performance of GPR is influenced by the EM properties of the soil, particularly with changes in moisture content (Das et al., 2001; Rhebergen et al., 2004; van Dam et al., 2004; Miller et al., 2004). Moreover, earlier researches have demonstrated how the detection uncertainty of GPR depends on the target features (van der Kruk et al., 2003; Daniels, 2004; Rhebergen and Ralston, 2005). Some studies have been carried out on the use of GPR for landmine detection in Colombia (Lopera et al., 2004, 2005). In these studies, measurements were taken using a 0.8 GHz time-domain GPR and it was concluded that an ultra-wide band (UWB) GPR would be more appropriate for landmine detection. Consequently, thorough studies are being performed with the aim of applying an UWB GPR for demining applications in Colombia (Lopera et al., 2007, 2007).

In this paper, we study the influences of soil and target characteristics in order to predict the detection performance of an UWB GPR for two representative mine-affected areas in Colombia. Accordingly, an EM model based on pedotransfer functions is coupled to a two-dimensional (2D), EM finite-difference time-domain (FDTD) GPR model so as to calculate target reflection responses for different environments. Firstly, typical AP landmines and IEDs and two types of soil from Colombian mine-affected areas are selected. Secondly, soil EM properties are derived using pedotransfer functions and available soil geophysical information. Finally, the GprMax FDTD model (Giannopoulos, 2002) is used for calculating the target signatures. The predicted performance shows how GPR could contribute to low- and non-metallic AP landmine detection in difficult soil conditions. Note that target detection is considered without taking into account target classification. To our knowledge, this paper constitutes a first contribution to a technological solution of demining issues in Colombia. The proposed methodology can be applied to other terrains and targets.

2. Materials and methods

2.1. Soil characteristics

Two ferruginous soils have been selected from two highly mine-affected departments of Colombia, located within The Andes mountain chain: Santander and Antioquia. The soils are classified as silt loam and loamy sand, respectively; their organic content is less than 1% and their reddish color is due to the presence of mixed oxides containing fine iron particles (their Fe percentage is 5.2% and 8.8%, respectively). These soils make the detection of low-metallic AP landmines using MDs more complicated (Toews and Sirovyak, 2003), due to their high magnetic susceptibility (MS, χ) and magnetic viscosity (or frequency-dependent MS, χ_{FD}) (Mullins, 1977). In order to determine the effect of the iron components on the EM properties, the magnetic susceptibility of the selected soils was measured using a Barington MS2 dual-frequency sensor (0.46/4.6 KHz) (Dearing, 1994). Several samples were taken from the upper 30 cm of the soil profile. Two measurements are obtained: the MS at low frequency (χ_{LF}) and the MS at high frequency (χ_{HF}). The frequency-dependent MS can therefore be expressed as a relative loss of susceptibility ($\chi_{FD}=\chi_{LF}-\chi_{HF}$) (Dearing et al., 1996). Results of these measurements and other available properties of both soils are summarized in Table 1.

[3] A low-metallic AP landmine is made with less than about 8 grams of iron or equivalent.

[4] Information source: http://www.derechoshumanos.gov.co/minas/.

Table 1
Available properties of the two ferruginous soils

Texture	Sand (%)	Silt (%)	Clay (%)	ρ_S (g/cm^3)	Θ_r (%)	Θ_s (%)	χ_{LF} (–)	χ_{HF} (–)	χ_{FD} (–)
Silt loam	30.6	63	6.4	1.18	4.4	38.9	307	304	2
Loamy sand	72.1	26.9	1	1.3	3.2	41	1080	1070	11

The residual water content (Θ_r) and the saturated water content (Θ_s) are calculated using the sand, silt and clay percentages and the bulk density (ρ_S) (Schaap et al., 1998). Several magnetic susceptibility measurements were made using a Barington dual-frequency sensor. We have only included the average values.

2.2. Target characteristics

The Colombian Army used AP landmines to protect telecommunications areas and Army bases until 1999.[5] Although these were mainly imported from the US (M14) and Belgium (NR-409), a few were produced by INDUMIL (MN-MAP-1, MN-MAP-2). All these are low-metallic content landmines and some of their features are summarized in Table 2. Usually, their case material is polyethylene (PE), polypropylene (PP), polystyrene (PS), rubber or bakelite, and their main charge is a mixture of different chemical components (see Table 2). Their dielectric constant ε_{tg} is calculated by averaging of the case material dielectric constant and the main charge dielectric constant, which values are taken from von Hippel (1995).

Mine-affected areas are also contaminated with IEDs, which cause 80% of the injuries by landmines in Colombia. These devices are not mass produced, they are fabricated in different forms, using different materials with a minimum or no metal content, which makes the detection of the non-metallic ones a challenging task. Some of their characteristics are summarized in Table 3. The size and shape of the IEDs can vary from a small piece of PVC ($\sim 10\times 14$ cm^2) to a large gas cylinder ($\sim 25\times 40$ cm^2). Additionally, some IEDs are fabricated with textile fiber and therefore, their shape is irregular. Usually, different kinds of explosives are used in the fabrication of IEDs. The most popular, and powerful, is known as ANFO (ammonium nitrate and fuel oil), although BENCLO (sodium benzoate and potassium chlorate) is also used. Besides the explosive, some devices are filled with tar (byproduct of petroleum) or a mix of tar and grapeshot (*e.g.*, nails).

[5] http://www.icbl.org/lm/2004/colombia.en.html.

Table 2
Summary of AP landmines features

Target	Diameter (cm)	Height (cm)	Material	Main charge[a]	d (cm)	ε_{tg} (–)
M14	5.6	4	Plastic	TETRYL	0–15	2.8
NR 409	8.2	2.8	Plastic	TNT+AAP+RDX	0–15	3.1
MN-MAP-1	7.5	7	Plastic	PETN+TNT+RDX	0–15	3.1

The burial depth d is measured from the top of the mine. The dielectric values are an average of the dielectric constants of the case material and of the main charge — values taken from von Hippel (1995).

[a] AAP = atomized aluminum powder, PETN = pentaerythrite tetranitrate, RDX = cyclotrimethylene trinitramine, TETRYL = trinitrophenyl, TNT = trinitrotoluene.

2.3. Calculation of the soil electromagnetic properties

The principal factor influencing the detection performance of GPR is the EM properties of the soil, namely, relative dielectric permittivity, ε, effective conductivity, σ_{eff} and magnetic permeability, μ. Although there are different approaches for modeling these properties, it is difficult to develop an opinion about the applicability of a method at a given environment because their success is dependent on the case study (Linde et al., 2006). In general, these methodologies are based on a-priori information, *i.e.*, different soil parameters previously measured which are introduced in to the model. It is important to clarify that the available data for a mine-affected area are limited, due to the impossibility of taking measurements in situ as well as the lack of geophysical data bases from mine-affected, underdeveloped countries. Since it is not within the scope of this paper to provide detailed

Table 3
Summary of some IED characteristics

Shape	Material	Geometry[a] (cm)	d (cm)	ε_{tg} (–)
Cylindrical	Metal	H=10–40, D=6–30	0–50	–
	PVC	H=10–17, D=8–14	0–10	3.6
	Wood	H=20–30, D=7–10	0–3	3.6/8.9
Rectangular	Wood	H=15–20, L=20–25, W=20–25	0–20	3.6/8.9
Irregular	Textile fiber	D=15–25	0–20	3.3

Plastic IEDs are made with polyvinylchloride or PVC. The textile fiber used for some IEDs is derived from the *fique* or *Furcraea macrophylla* plant. The burial depth d is measured from the top of the object. The dielectric values are an average of the dielectric constants of the case material and of the main charge — values taken from von Hippel (1995). Two values are provided for the wooden IEDs: dry and wet.

[a] H = Height, D = Diameter, L = Length, W = Width.

descriptions of all these approaches, we briefly describe some of them which could be applied in this case study. For more information about different approaches, the reader is referred to reviews given by Mavko et al. (1998), Lesmes and Friedman (2005), and the references therein.

Theoretical and empirical models of the electrical properties of the different components of the soil have been combined into semi-empirical models, which can be used to predict electrical properties of field soils. For this study, we require a model for predicting σ_{eff} as well as both the real and imaginary parts of ε ($\varepsilon=\varepsilon'-j\varepsilon''$) for a known frequency band and considering different moisture levels of a known soil type. In Toop et al. (1980), a semi-empirical model is proposed and relates the soil volumetric water content with ε. This approach is based on sandy soils and needs to be adjusted for each type of soil. This would require a calibrated formula for each environment, therefore we do not consider it for this study. Other semi-empirical models are based on mixing laws, such as the complex refracted index method (CRIM) (Tinga et al., 1973). In Shutko and Reutov (1982), it is demonstrated that CRIM gives a good approximation of ε for different soils in the range 1–10 GHz. However, it requires some parameters such as soil porosity which are not available in our case study. In Peplinski et al. (1995), a semi-empirical dielectric model based on pedotransfer functions (Gupta and Larson, 1979) is reported. This model relates the textural composition of the soil to electrical parameters and it covers the 0.3–1.3 GHz frequency range. The model provides frequency-dependent expressions for the real and imaginary parts of the relative dielectric constant of a soil medium in terms of the fraction of sand particles S, the fraction of clay particles C, the volumetric water content Θ and the bulk density of the soil ρ_S, all being available parameters. It is based on an earlier model for dielectric constants in the 1.4–18 GHz frequency range developed by Dobson et al. (1985). The real part of the complex relative dielectric permittivity for the bulk soil is approximated as

$$\varepsilon' = \left[1+\frac{\rho_S}{\rho_P}\left(\varepsilon_P^{\varphi}-1\right)+\Theta^{\beta'}\varepsilon'^{\varphi}_{fw}-\Theta\right]^{\frac{1}{\varphi}} \quad (1)$$

in Dobson et al. (1985), and

$$\varepsilon' = 1.15\left[1+\frac{\rho_S}{\rho_P}\left(\varepsilon_P^{\varphi}-1\right)+\Theta^{\beta'}\varepsilon'^{\varphi}_{fw}-\Theta\right]^{\frac{1}{\varphi}}-0.68 \quad (2)$$

in Peplinski et al. (1995). The imaginary part is derived as

$$\varepsilon'' = \left[\Theta^{\beta''}\varepsilon''^{\varphi}_{fw}\right]^{\varphi}, \quad (3)$$

where:

- ρ_P 2.66 g/cm^3 is a typical value,
- ε_P $(1.01+0.44\rho_P)^2-0.062$ is the empirical model of the dielectric constant of the soil particles,
- β' $127.48-0.519S-0.152C$ and,
- β'' $1.33797-0.603S-0.166C$ are two frequency independent constants which join the soil type into the model,
- φ 0.65 is empirically derived in Dobson et al. (1985) and Peplinski et al. (1995).

Furthermore, the frequency-dependent variables ε'_{fw} and ε''_{fw} are the real and imaginary parts, respectively, of the dielectric constant for free water. The latter depends on the effective conductivity, σ_{eff}, which is derived in Dobson et al. (1985) as

$$\sigma_{\text{eff}} = 1.645+1939\rho_S-2.25622S+1.549C, \quad (4)$$

and in Peplinski et al. (1995) as

$$\sigma_{\text{eff}} = 0.0467+0.2204\rho_S-0.4111S+0.6614C. \quad (5)$$

Once ε is approximated using the proposed semi-empirical models, other factors influencing the detection performance of GPR can be derived. They are the attenuation factor α and the dielectric permeability contrast $\varepsilon_{\text{contrast}}$. The attenuation factor α, in dB, depends on the magnetic permeability of the soil, $\mu=\mu_0+\mu_0\chi_{FD}$ ($\mu_0=4\pi*10^{-7}$ H/m), the complex permittivity of the soil and the angular frequency of the radar wave, ω, (Reynolds, 1998). It is derived from the equation

$$\alpha = \omega\sqrt{\frac{\mu\varepsilon_{\text{eff}}}{2}\left[\sqrt{1+\left(\frac{\varepsilon''}{\varepsilon'}\right)^2}-1\right]}, \quad (6)$$

where $\varepsilon_{\text{eff}}=\varepsilon'\varepsilon_0$ is the effective permittivity of soil ($\varepsilon_0=8.85*10^{-12}$ F/m) and the ratio between ε'' and ε' is commonly referred to as the loss factor or loss tangent. This equation is only valid when $\mu\leq 1$, which is the case for both soils. Assuming a plane wave vertically incident on the top of the target, the dielectric permeability contrast $\varepsilon_{\text{contrast}}$ between the target and the

background is calculated according to (Reynolds, 1998):

$$\varepsilon_{\text{contrast}} = \frac{\sqrt{\varepsilon} - \sqrt{\varepsilon_{\text{tg}}}}{\sqrt{\varepsilon} + \sqrt{\varepsilon_{\text{tg}}},} \quad (7)$$

where ε_{tg} is the relative dielectric permittivity of the target, which imaginary part is considered as zero.

Since the strength of the buried target reflection depends on the wave penetration and the dissimilarity between soil and target permittivity, α and $\varepsilon_{\text{contrast}}$ have a direct impact on the signal-to-noise ratio (SNR), as it is pointed out further in the following section.

2.4. Modeling ground-penetrating radar

All electromagnetic phenomena, on a macroscopic scale, are described by Maxwell's equations. These are first-order partial differential equations that mathematically express the relationship between the fundamental electromagnetic field quantities and their dependence on their sources (Balanis, 1989). In order to simulate the GPR response from a particular target or set of targets embedded in the soil, these equations have to be solved subject to the geometry of the problem and its initial conditions. One of the available numerical programs for computing GPR wave propagation and signal properties is GprMax (Giannopoulos, 2002), which solves Maxwell's equations using the finite-difference time-domain, FDTD, method (Taflove, 1995). FDTD techniques are based on discretizing both space and time using an orthogonal grid and solving the differential form of Maxwell's equations employing a second or fourth order approximation. An example of the numerical domain modeled with this tool is shown in Fig. 1.

In this numerical simulation, a specific GPR configuration is modeled. Firstly, a monostatic UWB GPR is selected to avoid coupling between the transmitting and receiving antennas. This eliminates an important unwanted signal artefact that may obscure the other information in the signal. Secondly, the transmitting/receiving antenna is located over the soil surface at a maximal height of 20 cm. This value is a practical optimum that allows high antenna mobility without increasing the spreading loss. Finally, the choice of the bandwidth depends on the desired depth resolution and signal penetration. At frequencies above 1 GHz, depth penetration decreases dramatically (Daniels, 2004), whereas resolution increases. On top of this, one has to deal with rough surfaces and soil attenuation for shorter wavelengths (Sai and Ligthart, 2004). The frequency range 0.8–2.8 GHz is selected because it is in the range of most landmine GPR applications. Additionally, the size of the targets is larger than the wavelength of the propagating GPR wave (under the conditions considered here), therefore the target backscattering should be significant.

3. Results and discussion

3.1. Estimation of the dielectric permittivity, attenuation and dielectric contrast

For frequencies ranging between 0.8 GHz and 2.8 GHz and for the two types of soil, the complex relative dielectric permittivity is approximated using Eqs. (1)–(3). Note that they depend on Eqs. (4) and (5).

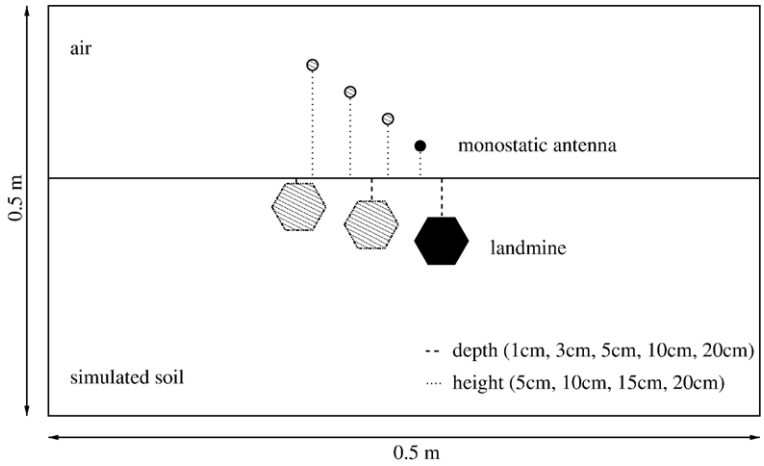

Fig. 1. Numerical domain used in the FDTD program.

Different water content fractions are selected, which range between the residual water content, Θ_r, and the saturated water content, Θ_s (see Table 1). In Fig. 2, the estimated real and imaginary values of ε for the silt loam and loamy sand soil are shown as a function of the frequency (at 10% water content), and as a function of the water content (at 0.8 GHz and 2.5 GHz).

Considering the empirical model, different values of the real and imaginary parts of ε are found in Fig. 2 (A and B) for frequencies below and above 1.4 GHz,

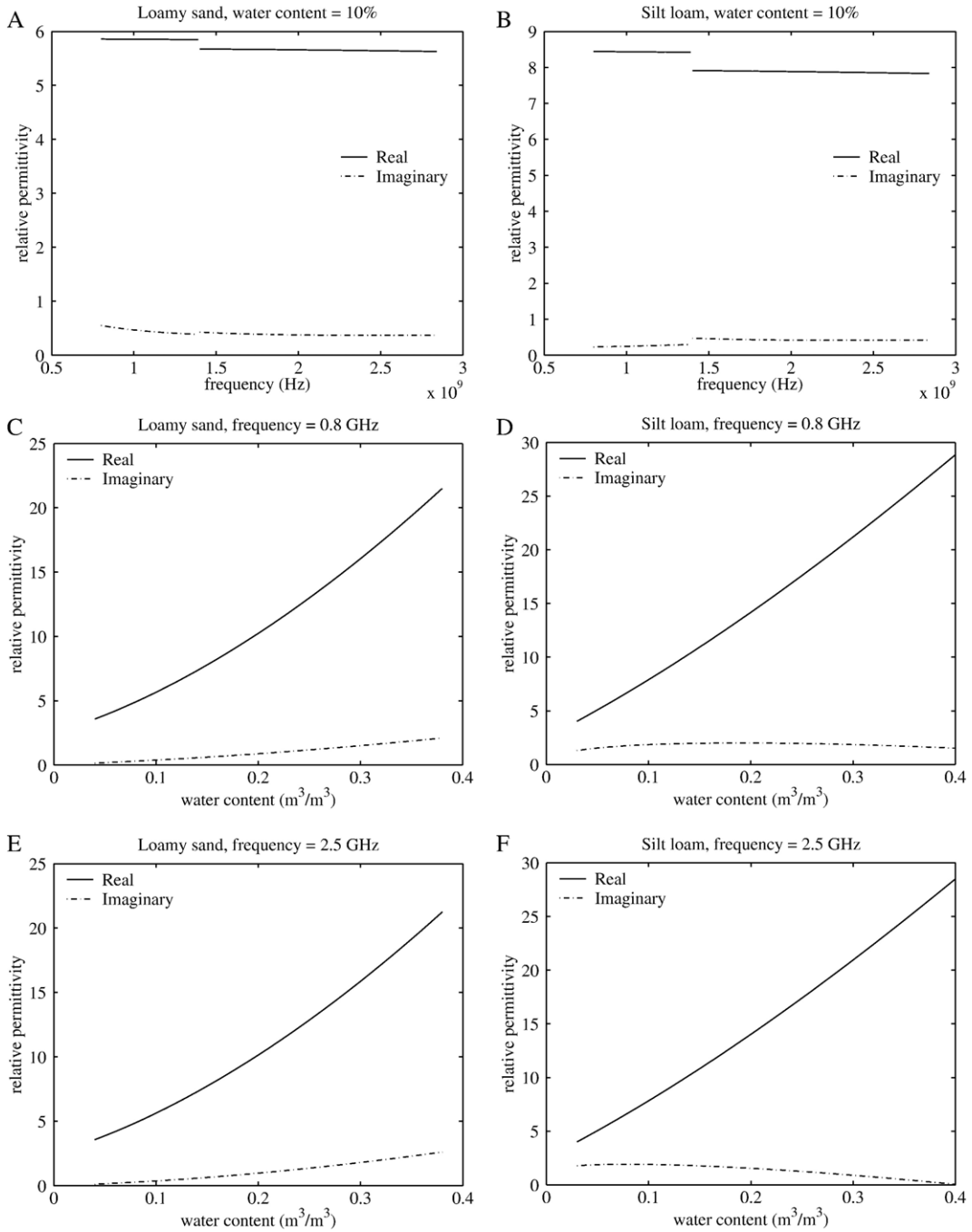

Fig. 2. Examples of the complex relative dielectric permittivity calculated for both soils as a function of: (A and B) frequency, at 10% of water content, (C and D) water content, at 0.8 GHz, and (E and F) water content, at 2.5 GHz. Results of the silt loam soil are in the left column and those of the loamy sand soil are in the right column.

and the same occurs at all different water content fractions. In practice, the dependence of the dielectric permittivity on the frequency should be a continuous function. For the estimated values, the maximum difference in ε is no more than 0.04. This value is lower than the error values found in Peplinski et al. (1995), after the linear adjustment introduced to correct the model reported in Dobson et al. (1985). Additionally, similar errors on the estimated values of the real and imaginary parts of ε are observed in Ponizovsky et al. (1999) and Yu et al. (1999). Since these studies compare experimental results with predictions based on other empirical models, one can state that such a difference should not represent a relevant error. Therefore, we can expect that this small gap on the representation of ε will have a slight impact on the simulations. Nevertheless, it would be interesting to compare these estimated values with experimental results.

In Fig. 2 (C–F) one can observe that the real part of ε of both soils increases as the water content increases. Other interesting results are obtained for the imaginary part. In the loamy sand case, the latter hardly increases, whereas it decreases in the silt loam case. Since ε'' is related to losses (loss tangent), it has an important impact on the attenuation. For a specific frequency, the higher ε'', the more important the attenuation degree. This effect is illustrated by solving Eq. (6). In the loamy sand soil, α increases as water content increases, whereas α of the silt loam soil decreases as water content increases, and the same occurs at all frequencies.

The dielectric contrast is calculated for all different values of the target relative dielectric permittivity, ε_{tg} (see Tables 2 and 3), different water content fractions between the residual water content, Θ_r, and the saturated water content, Θ_s, as well as different frequencies between 0.8 GHz and 2.8 GHz. At all fractions of water content, $\varepsilon_{contrast}$ for frequencies below 1.4 GHz is a little larger than $\varepsilon_{contrast}$ for frequencies above 1.4 GHz, which is a logical expectation, considering the empirical formulae. In accordance with Eq. (7), $\varepsilon_{contrast}$ increases as water content increases, due to a larger difference between ε and ε_{tg}.

In Table 4, columns 3, 4 and 5 summarize ε', α and $\varepsilon_{contrast}$, respectively, for three different water contents, 10%, 20% and 30%, at 1.8 GHz, and for three different ε_{tg} (or three different targets), 2.8 (*e.g.*, M14), 3.3 (*e.g.*, IED fabricated with textile fiber) and 3.6 (*e.g.*, IED fabricated with PVC).

3.2. Numerical modeling of GPR

Simulations are carried out following different configurations of the numerical domain of Fig. 1. Firstly, eight types of target, with different shape and ε_{tg}, are represented at several depths, between 1 cm and 20 cm. Secondly, the transmitting/receiving point is placed at four different heights, between 5 cm and 20 cm. Additionally, three water contents are considered, between Θ_r and Θ_s, and the constitutive parameters (μ, ε' and σ_{eff}) describing both soils at such moisture levels are introduced into the model. The combination of all these attributes leads to a great number of configurations. Although results are shown and discussed in this section for some of them, the observations stated below can be extended to all results.

Fig. 3 (A and B) represent the simulated GPR scans for a M14 AP landmine buried at 3 cm in the silt loam and the loamy sand soil, respectively. The transmitting/receiving point is placed at 5 cm above the soil surface. It is excited using a Ricker wavelet, which has a peak amplitude of 1.0 A and a central frequency of 1.8 GHz. In the silt loam soil, the amplitude of the numerical signal increases as soil water content increases, whereas it decreases as soil water content increases in the loamy sand soil. Therefore, the predicted effect of the attenuation factor using Eq. (6) is validated by the numerical simulations.

In Fig. 3 (C–F), the amplitude of the simulated target response for a M14 AP landmine buried in both soils

Table 4
Results of the approximated values (ε', α and $\varepsilon_{contrast}$) for the two types of soil under three water content fractions and different targets (1: M14 AP mine, 2: textile fiber IED, 3: PVC IED)

Soil	WC (%)	ε' (–)	α (dB)	$\varepsilon_{contrast1}$ (dB)	$\varepsilon_{contrast2}$ (dB)	$\varepsilon_{contrast3}$ (dB)	SNR_1 (dB)	SNR_2 (dB)	SNR_3 (dB)
Silt loam	10	7.7	−14.5	−15.1	−17.3	−18.8	−26	−22.3	−19.5
Silt loam	20	14.1	−19	−10	−11.1	−11.8	−23.7	−24.9	−21
Silt loam	30	21.4	−21.8	−7.7	−8.4	−8.9	−17.8	−19.2	−18.1
Loamy sand	10	5.7	−28.7	−11.5	−12.9	−13.7	−16.1	−18.1	−14.9
Loamy sand	20	10.5	−25.8	−8.2	−9	−9.5	−25.4	−25.4	−23.3
Loamy sand	30	16.5	−21.5	−6.5	−7.2	−7.5	−30.3	−32.2	−31.2

The SNR for the targets buried at 5 cm of depth, with the antenna placed at 5 cm above the soil surface, are also given.

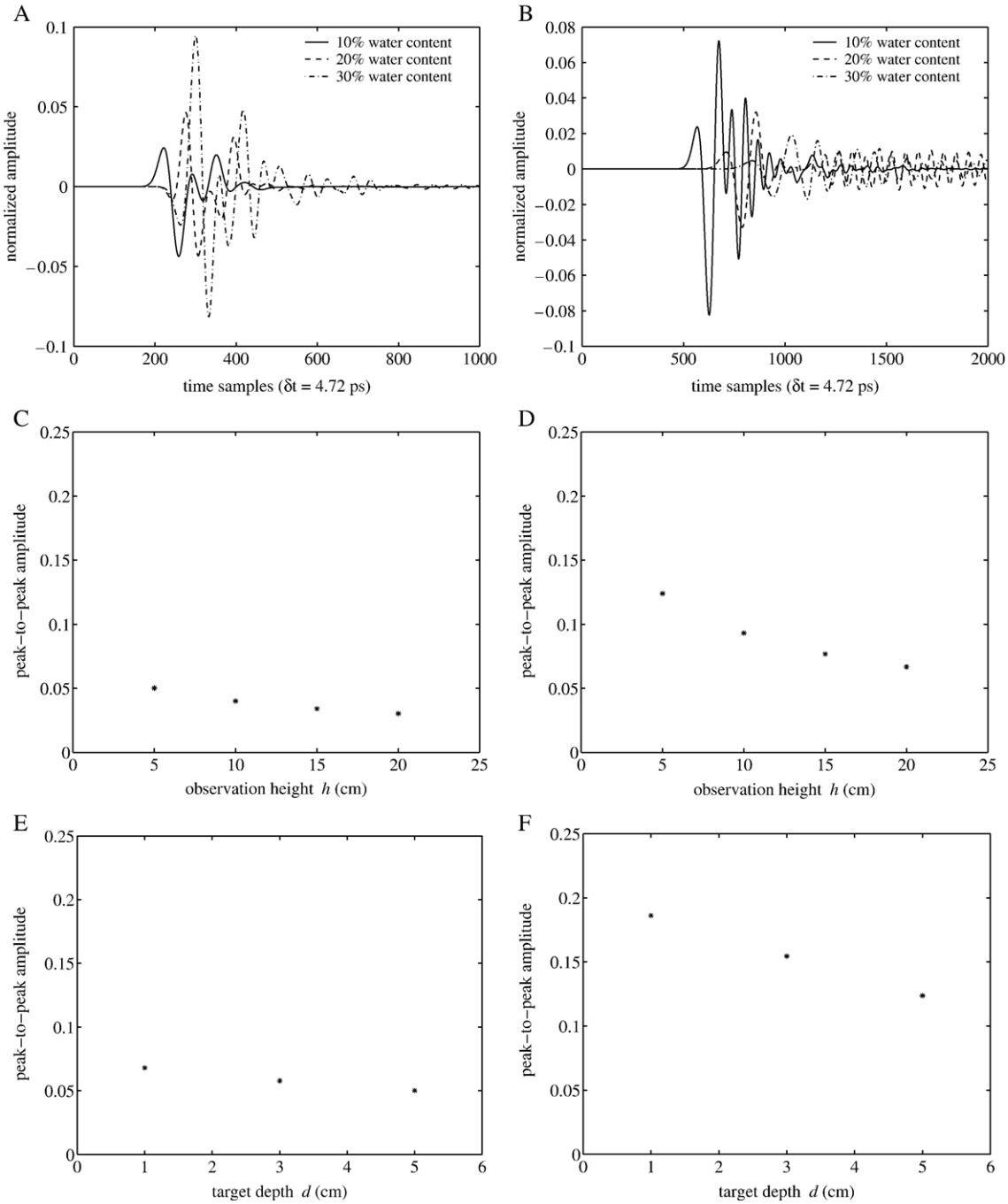

Fig. 3. Representations of the simulated signal amplitude of a M14 AP landmine as a function of: (A and B) time and water content, at 1.8 GHz, (C and D) observation height, at 1.8 GHz and 10% of water content, and (E and F) target depth, at 1.8 GHz and 10% of water content. Results of the silt loam soil are in the left column and those of the loamy sand soil are in the right column.

(10% of water content) is shown as a function of the antenna height and target depth. In the silt loam soil, the signal amplitude barely decreases as target depth and antenna height increase, which is a consequence of the weak attenuation. In the loamy sand soil, the strong attenuation leads to a rapid decrease of the signal amplitude when the target depth and the antenna height increase.

Interesting observations can be made on the effect of α and $\varepsilon_{contrast}$ on the SNR for different fractions of water

content. In the loamy sand soil, as the water content increases, $\varepsilon_{contrast}$ increases. However, α increases and, therefore the SNR decreases. This is not the case in the silt loam soil. For the latter, as the water content increases, α decreases and $\varepsilon_{contrast}$ increases, therefore the SNR increases. This effect is summarized in the three last columns of Table 4 for three targets: 1) M14, 2) IED fabricated with textile fiber, and 3) IED fabricated with PVC. They are located at a depth of 5 cm and the antenna is placed at 5 cm above the surface. From these results, we can observe that the target shape also influences the SNR. Irregular objects, such as target 2, will negatively affect the SNR, whereas larger, more regular objects, such as targets 1 and 3, will have a better SNR. As expected, the models show that the deeper the objects are buried and the higher the antennas are placed, the weaker the SNR will be (results not shown in the table).

From the simulations one can state that deeper objects (*e.g.* 15 cm) will be hardly detected in both soils by a monostatic GPR working in the 0.8–2.8 GHz bandwidth, especially when the antenna is placed higher than 5 cm. Additionally, in the loamy sand soil, such GPR systems will perform better in dry conditions (*e.g.*, water content $\approx$ 10%), contrary to the silt loam soil. For the latter, the attenuation factor will become weaker as the soil water content increases and therefore, as the contrast between the soil and the target increases, the GPR will perform better in wet conditions (*e.g.*, water content $\approx$ 30%). Considering a smooth surface and a homogeneous soil, the backscattered signal from low-metallic AP landmines and non-metallic IEDs will have a higher SNR under these conditions than under other configurations. Rough surfaces and heterogeneous soils constitute an additional source of clutter, therefore the SNR is reduced. Following the recommendations in Yarovoy et al. (2003), and in addition to the GPR characteristics considered here, a high linear dynamic range GPR (*e.g.* −60 dB) should be used for increasing the possibility of detecting a buried target where the backscattered signal is obscured by such additional clutter.

4. Summary and conclusions

An existing EM model, based on pedotransfer functions, is coupled to a 2D EM FDTD model to predict the effects of soil and target properties on the detection performance of GPR. Soil magnetic properties and soil textural class are previously measured and determined. They are included in pedotransfer functions in order to estimate the frequency-dependent electrical properties of soil. The latter are used for simulating buried target backscattered signal using the GprMax FDTD code, for different fractions of water content and different configurations of the antenna height and target depth. The analysis of the results allows us to determine the influence of the EM properties of soil, as well as that of the target characteristics, on the GPR detection performance.

Prediction of the effects of soil and target properties on the detection performance of GPR is focused on two representative mine-affected soils in Colombia. Different fractions of water content, as well as AP landmines and local explosive devices, are considered. From the estimated EM values, the attenuation factor and dielectric contrast are calculated. The effects of such parameters on the SNR are validated by the simulations.

Although there are some omitted influencing factors in our approach, such as a rough surface or heterogeneous soil, one can predict from the results favorable scenarios for landmine detection using a monostatic GPR in the 0.8–2.8 GHz frequency band. Such a system, with a high linear dynamic range, could be quite adequate for complementing humanitarian landmine detection by metal detectors in the selected environments. The methodology presented here can be applied to other types of soil and targets for predicting GPR detection performance (note that, in this paper, we are referring to only object detection. A posteriori process needs to be performed to identify and classify the detected target as a mine-like object or as a friendly object). However, a comparison with laboratory and in situ measurements should be carried out in order to determine the relevancy of the error introduced by the gap in the dielectric permittivity estimated using the models of Dobson et al. and Peplinski et al.

Acknowledgments

This research project is carried out at the Signal and Image Centre of the Royal Military Academy, Belgium, and at the Electrical and Electronic Dept. of the University of Los Andes, Colombia, in collaboration with the Telecommunications Laboratory, Catholic University of Louvain, Belgium. It is supported by the Ministry of Defence of Belgium, in the scope of the BEMAT project, and by the Colombian Institute for the Development of Science and Technology. The authors would like to thank the Colombian Military Forces for their support, specially the personnel of the MARTE group and the BAMAI laboratory, as well as Dr. S. Lambot and two anonymous reviewers, for valuable discussions and their constructive comments to the manuscript.

References

Balanis, C.A., 1989. Advanced Engineering Electromagnetics. John Wiley & Sons, Inc., New York.

Bruschini, C., Gros, B., Guerne, F., Pice, P., Carmona, O., 1998. Ground penetrating radar and imaging metal detector for antipersonnel mine detection. Journal of Applied Geophysics 40, 59–71.

Carin, L., Geng, N., McClure, M., Sichina, J., Nguyen, L., 1999. Ultra-wide band synthetic-aperture radar for mine-field detection. IEEE Antennas and Propagation Magazine 41, 18–33.

Chen, C., Rao, K., Lee, R., 2001. A tapered-permittivity rod antenna for ground penetrating radar applications. Journal of Applied Geophysics 47, 309–316.

Daniels, D., 2004. Surface Penetrating Radar, 2nd edition. The Inst. Electrical Eng., London.

Das, B., Hendrickx, J., Borchers, B., 2001. Modeling transient water distributions around landmines in bare soils. Journal of Soil Science 166, 163–173.

Dearing, J., 1994. Environmental Magnetic Susceptibility: Using the Bartington MS2 System. Chi Publishing, Kenilworth.

Dearing, J., Dann, R., Hay, K., Lees, J., Loveland, P., Maher, B., O'Grady, K., 1996. Frequency-dependent susceptibility measurements of environmental materials. Geophysical Journal International 124, 228–240.

Dobson, M., Ulaby, F., Hallikainen, M., El-Rayes, M., 1985. Microwave dielectric behavior of wet soil — Part II: dielectric mixing models. IEEE Transactions on Geoscience and Remote Sensing 23, 35–46.

Gao, P., Collins, L., Garber, P., Geng, N., Carin, L., 2000. Classification of landmine-like metal targets using wideband electromagnetic induction. IEEE Transactions on Geoscience and Remote Sensing 38, 1352–1361.

Giannopoulos, A., 2002. GprMax2D/3D V1.5 User Manual. University of Edinburgh, Edinburgh.

Gupta, S., Larson, W., 1979. Estimating soil water retention characteristics from particle size distribution, organic matter percent and bulk density. Water Resources Research 25, 1633–1635.

ICBL, 2005. Landmine Monitor Report 2005, Toward a Mine-free World. Human Rights Watch, Washington D.C.

Lesmes, D., Friedman, S., 2005. Relationships between the electrical and hydrogeological properties of soils and rocks. Hydrogeophysics 87–128.

Linde, N., Chen, J., Kowalsky, M., Hubbard, S., 2006. Hydrogeophysical parameter estimation approaches for field scale characterization. Applied Hydrogeophysics. Springer, London. Chap 2.

Lopera, O., Milisavljevic, N., Macq, B., van den Bosch, I., Lambot, S., Gauthier, A., 2004. Analysis of segmentation techniques for landmine signature extraction from Ground Penetrating Radar 2D data. In: IEEE (Ed.), eProceedings of the II International IEEE Andean Region Conference. Bogota, Colombia. ISBN: 958-33-6534-3. p. on CD.

Lopera, O., Macq, B., Milisavljevic, N., Scheers, B., 2005. Denoising and migration techniques for landmine identification from ground-penetrating radar 2D data. In: UCL-FSA (Ed.), eProceedings of GRETSI 2005. Louvain-la-neuve, Belgium. p. on CD.

Lopera, O., Milisavljevic, N., Lambot, S., 2007. Clutter reduction in GPR measurements for detecting shallowly buried landmines: a Colombian case study. Near Surface Geophysics 5, 73–80 (February).

Lopera, O., Slob, E., Milisavljevic, N., Lambot, S., 2007. Filtering soil surface and antenna effects from GPR data to enhance landmine detection. IEEE Transactions on Geoscience and Remote Sensing 45 (3), 707–717.

MacDonald, J., Loockwood, J., Altshuler, T., Broach, T., Carin, L., Harmon, R., Rappaport, C., Scott, W., Weaver, R., 2003. Alternatives for Landmine Detection. RAND, USA.

Mavko, G., Mukerji, T., Dvorkin, J., 1998. The Rock Physics Handbook. Cambridge University Press, UK.

Miller, T., Hendrickx, J., Borchers, B., 2004. Radar detection of buried landmines in field soils. Vadose Zone Journal 3, 1116–1127.

Mullins, C., 1977. Magnetic susceptibility of the soil and its significance in soil science — a review. Journal of Soil Science 28, 223–246.

Peplinski, N., Ulaby, F., Dobson, M., 1995. Dielectric properties of soils in the 0.3–1.3 GHz range. IEEE Transactions on Geoscience and Remote Sensing 33, 803–807.

Ponizovsky, A.A., Chudinova, S.M., Pachepsky, Y.A., 1999. Performance of TDR calibration models as affected by soil texture. Journal of Hydrology 218, 35–43.

Reynolds, J., 1998. An Introduction to Applied and Environmental Geophysics. John Wiley and Sons, New York.

Rhebergen, J.B., Ralston, J., 2005. Test and evaluation protocols for GPR-based mine-detection systems; a proposal. In: SPIE (Ed.), Detection and Remediation Technologies for Mines and Mine-like Targets X. Orlando, FL, pp. 941–952.

Rhebergen, J.B., Lensen, H.A., van WijK, R., Hendrickx, J.M.H., van Dam, L., Borchers, B., 2004. Prediction of soil effects on GPR signatures. In: SPIE (Ed.), Defence and Security Symposium. Orlando, FL, pp. 705–715.

Roth, F., 2004. Convolutional models for landmine identification with ground penetrating radar. Ph.D. thesis, Delft University of Technology, Delft, The Netherlands.

Sai, B., Ligthart, L., 2004. GPR phase-based techniques for profiling rough surfaces and detecting small, low-contrast landmines under flat ground. IEEE Transactions on Geoscience and Remote Sensing 42, 318–418.

Schaap, M., Leij, F., van Genuchten, M., 1998. Neural network analysis for hierarchical prediction of soil water retention and saturated hydraulic conductivity. Soil Science Society of America Journal 62, 847–855.

Scheers, B., 2001. Ultra-wideband ground penetrating radar with application to the detection of anti personnel landmines. Ph.D. thesis, Catholic University of Louvain — Royal Military Academy, Belgium.

Shutko, A., Reutov, E., 1982. Mixture formulas applied in estimation of dielectric and radiative characteristics of soils and grounds at microwave frequencies. IEEE Transactions on Geoscience and Remote Sensing 20, 29–32.

Taflove, A., 1995. Computational Electrodynamics —The Finite Difference Time Domain method. Artech House, London.

Tinga, W., Voss, W., Blossey, D., 1973. Generalized approach to multiphase mixing theory. Journal of Applied Physics 44, 3897–3902.

Toews, J., Sirovyak, W., 2003. Metal detector trial — Colombia: technical memorandum. Defence R&D Canada, TM 2003-099, Colombia.

Toop, G.C., Davis, J.L., Annan, A., 1980. Electromagnetic determination of soil water content: measurements in coaxial transmission lines. Water Resources Research 16, 574–582.

van Dam, R., Borchers, B., Hendrickx, M., 2004. Strength of landmine signatures under different soil conditions: implications for sensor fusion. System Science 36 (9), 573–588.

van der Kruk, J., Wapenaar, C., Fokema, J., van der Berg, P., 2003. Three-dimensional imaging of multi-component ground penetrating radar data. Geophysics 57, 1241–1254.

von Hippel, A., 1995. Dielectric Materials and Applications. Artech House.

Yarovoy, A., Kovalenko, V., Fogar, A., 2003. Impact of clutter on buried object detection by ground penetrating radar. International Geoscience and Remote Sensing Symposium. France, pp. 755–757.

Yu, C., Warric, A.W., Conklin, M.H., 1999. Derived functions of time domain reflectometry for soil moisture measurement. Water Resources Research 35, 1789–1796.